5-1-2014

Spectroscopic and Mechanistic Studies of Heterodimetallic Forms of Metallo-β-lactamase NDM-1

Hao Yang
Miami University - Oxford

Mahesh Aitha
Miami University - Oxford

Amy R. Marts
Miami University - Oxford

Alyssa Hetrick
Miami University - Oxford

Brian Bennett
Marquette University, brian.bennett@marquette.edu

See next page for additional authors

Published version. *Journal of the American Chemical Society,* Vol. 136, No. 20 (May 2014): 7273–7285. DOI.

JACS
JOURNAL OF THE AMERICAN CHEMICAL SOCIETY
Article
pubs.acs.org/JACS

Spectroscopic and Mechanistic Studies of Heterodimetallic Forms of Metallo-β-lactamase NDM-1

Hao Yang,[†] Mahesh Aitha,[†] Amy R. Marts,[†] Alyssa Hetrick,[†] Brian Bennett,[‡] Michael W. Crowder,[†] and David L. Tierney*[,†]

[†]Department of Chemistry and Biochemistry, Miami University, Oxford, Ohio 45056, United States
[‡]Department of Biophysics, Medical College of Wisconsin, Milwaukee, Wisconsin 53226, United States

Supporting Information

ABSTRACT: In an effort to characterize the roles of each metal ion in metallo-β-lactamase NDM-1, heterodimetallic analogues (CoCo-, ZnCo-, and CoCd-) of the enzyme were generated and characterized. UV−vis, ^{1}H NMR, EPR, and EXAFS spectroscopies were used to confirm the fidelity of the metal substitutions, including the presence of a homogeneous, heterodimetallic cluster, with a single-atom bridge. This marks the first preparation of a metallo-β-lactamase selectively substituted with a paramagnetic metal ion, Co(II), either in the Zn_1 (CoCd-NDM-1) or in the Zn_2 site (ZnCo-NDM-1), as well as both (CoCo-NDM-1). We then used these metal-substituted forms of the enzyme to probe the reaction mechanism, using steady-state and stopped-flow kinetics, stopped-flow fluorescence, and rapid-freeze-quench EPR. Both metal sites show significant effects on the kinetic constants, and both paramagnetic variants (CoCd- and ZnCo-NDM-1) showed significant structural changes on reaction with substrate. These changes are discussed in terms of a minimal kinetic mechanism that incorporates all of the data.

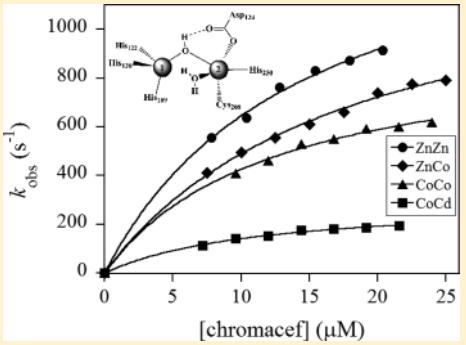

INTRODUCTION

β-Lactam-containing antibiotics that target bacterial cell wall synthesis, such as penicillins, cephalosporins, and carbapenems, remain the cheapest and some of the most effective antimicrobial agents available,[1] representing more than 50% of the antibiotics prescribed worldwide. The selective pressure applied by their wide and extensive application has resulted in resistance,[2] conferred by the production of β-lactamases. More than 1,000 β-lactamases have been isolated, and these enzymes have been categorized into four classes based on amino acid sequence.[1,3] Classes A, C, and D, also known as the serine-β-lactamases (SβLs), use an active site serine to perform nucleophilic attack on the β-lactam carbonyl, forming a covalent enzyme−substrate adduct, and these enzymes generally display very narrow substrate profiles, although examples of SβLs with broad activity have recently been reported.[4,5] In contrast, Class B β-lactamases, also known as the metallo-β-lactamases (MβLs), require either 1 or 2 equiv of Zn(II) for full catalytic activity, and these enzymes hydrolyze all clinical β-lactam-containing compounds. The MβLs have been further divided into subclasses B1−B3, based on sequence homology.[6]

Although SβLs are more clinically prevalent than MβLs, they remain sensitive to an array of mechanism-based inhibitors, such as clavulanic acid, sulbactam, and tazobactam. The MβLs are generally insensitive to SβL inhibitors, and no clinical inhibitors exist for these enzymes. A number of clinically important bacterial strains have been reported to produce chromosomally encoded MβLs, such as *Bacillus cereus* (BcII),[7] *Bacteroides fragilis* (CcrA),[8] *Elizabethkingia meningoseptica* (BlaB),[9] and *Stenotrophomonas maltophilia* (L1).[10] Several plasmid-encoded MβLs, such as IMP[11] and VIM[12] variants, have been shown to horizontally transfer to other pathogenic bacteria. NDM-1 was initially discovered in *Klebsiella pneumonia*. Like bla_{IMP-1} and bla_{VIM-1}, bla_{NDM-1} has been shown to be horizontally transferable.[13] Clinical strains of *Enterobacteriaceae* and *A. baumannii* now harbor the bla_{NDM-1} gene.[14−16] IMP, VIM, and NDM are all class B1 MβLs, by far the most abundant and clinically relevant subclass of the MβLs.[17−19]

The native Zn(II)-containing MβLs are accessible only by X-ray crystallography and X-ray absorption spectroscopy (XAS). Substitution of the active site Zn(II) with Co(II) is a common practice, as it makes the enzymes amenable to NMR, EPR, and UV−vis spectroscopies, allowing for more detailed structural and mechanistic studies. However, as all known examples of B1 MβLs bind 2 equiv of divalent metal tightly, spectroscopic signatures from fully substituted enzymes are difficult to assign to specific metal sites (Zn_1 or Zn_2, Figure 1; for clarity, we will refer to all metal-substituted variants in numerical order, that is, ZnCo refers to Zn(II) in the Zn_1 site and Co(II) in the Zn_2 site). While heterodimetallic forms are desirable, well-characterized examples are relatively few. Vila and co-workers first reported spectroscopic studies on a mixed-metal (ZnCo) form of BcII.[20] More recently, we reported spectroscopic studies on the ZnCo form of the B3 MβL L1.[21] However, structural and catalytic features specific to the Zn_1 site cannot be established without a

Received: October 9, 2013
Published: April 23, 2014

   dx.doi.org/10.1021/ja410376s | J. Am. Chem. Soc. 2014, 136, 7273−7285

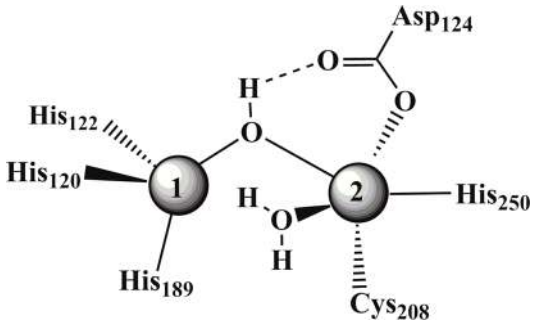

Figure 1. Active site structure of NDM-1 based on the current spectroscopic studies, with the ligand arrangement based on the X-ray structure of NDM-1 (Strynadka, *et al.*).[50]

complementary form of the enzyme that incorporates a paramagnetic metal ion in the Zn_1 site and a diamagnetic metal ion in the Zn_2 site.

We report here the preparation, characterization, and mechanistic investigation of several heterodimetallic forms of the MβL NDM-1, in an effort to establish the functional roles of each metal ion. The reaction of these mixed-metal forms with chromacef was followed using rapid-freeze-quench (RFQ) EPR, allowing a detailed assessment of the coordination environment of each metal binding site, independently, during the formation and decay of a key ring-opened reaction intermediate that is commonly formed by most MβLs with chormacef or nitrocefin as substrate (a similar intermediate has been reported in the reaction of BcII with penicillin[22] and imipenem[23]). The minimal reaction mechanism developed here is discussed in light of the available data on NDM-1, both reported previously[19,24] and herein.

EXPERIMENTAL PROCEDURES

Materials. *Escherichia coli* strains DH5a and BL21(DE3) were purchased from Novagen (Madison, WI). Restriction enzymes, *Nde*I and *Xho*I, were purchased from New England Biolabs. Luria−Bertani (LB) medium was purchased from Invitrogen (Carlsbad, CA). Isopropyl-β-D-thiogalactoside (IPTG) was purchased from Anatrace (Maumee, OH). Chromacef was purchased from Sopharmia, Inc. All buffer solutions and growth media were made with Barnstead NANOpure water. Kinetic and spectroscopic studies were conducted in 50 mM HEPES (pH 7.0) containing 200 mM NaCl and 1 mM TCEP [tris(2-carboxyethyl)phosphine] (referred to simply as "buffer" from here). All dialyses were performed against buffer containing 10 mM EDTA ("chelation buffer"), 12 h per buffer volume.

Preparation of apo-, CoCo-, ZnCo-, and CoCd-NDM-1. NDM-1 was expressed and purified as described previously.[19] Protein concentrations were determined using the extinction coefficient at 280 nm, ε_{280} = 28,500 M^{-1} cm^{-1}. To prepare apo-NDM-1, the purified enzyme (ca. 300 μM) was dialyzed at 4 °C against 3 × 1 L of chelation buffer. EDTA was removed by dialysis against 6 × 1 L of buffer. CoCo-NDM-1 was prepared by titrating 300 μM apo-NDM-1 with Co(II) in buffer. The mixed-metal hybrids were prepared by incubating 300 μM apoenzyme, with 1 equiv of the diamagnetic metal from a 10 mM stock solution in buffer, followed by addition of Co(II), also from a 10 mM stock. For example, ZnCo-NDM-1 was prepared by incubating the apoenzyme with 1 equiv of Zn(II) on ice for 30 min, followed by titration with Co(II). The CoCd enzyme was prepared in a similar fashion, by incubation of the apoenzyme with 1 equiv of Cd(II), followed by the addition of 1 equiv of Co(II).

Steady-State Kinetics. Steady-state kinetic studies were performed using 50 nM enzyme at 9 °C, unless otherwise noted, on a Hewlett-Packard 5480A diode array spectrophotometer. The hydrolysis of chromacef by ZnZn-, CoCo-, ZnCo-, and CoCd-NDM-1 was monitored by detecting the formation of product at 442 nm, and absorbance data were converted into concentrations using $\Delta\varepsilon_{442}$ = 18,600 M^{-1} cm^{-1}. Kinetic studies were carried out in buffer, with substrate concentrations that varied from 1 to 100 μM. The initial rate of product formation *vs* substrate concentration was fit to the Michaelis−Menten equation to determine the steady-kinetic constants, K_m and $k_{cat.}$

NMR Spectroscopy. ^{1}H NMR spectra were collected on 2 mM samples of metal-substituted NDM-1 in buffer containing ~10% D_2O. Exchangeable protons were identified by comparison with samples in ~90% D_2O. ^{1}H NMR spectra were recorded at 290 K on a Bruker ASX200 spectrometer operating at 200.13 MHz. Data were collected using a frequency switching technique that places a long, low-power (saturating) pulse on the water signal, before moving the transmitter to an arbitrary region of interest.[25] This approach allows accentuation of severely hyperfine-shifted resonances and often more uniform excitation. Spectra for NDM-1 collected in this manner were the average of ~200,000 transients consisting of 8k points over a 75 kHz spectral window (t_{AQ} = 54 ms, total data collection took approximately 16 h per spectrum). The presaturation pulse was typically 100−150 ms (~1 W), centered at the water frequency, while the acquisition pulse was 3 μs at full power, typically centered between +50 and +200 ppm. Prior to Fourier transformation, all FIDs were apodized using an exponential function that introduced an additional line width of 30 Hz (0.15 ppm).

EXAFS Spectroscopy. Samples for EXAFS (approximately 1 mM in protein) were prepared with 20% (v/v) glycerol as a glassing agent. EXAFS samples were loaded in Lucite cuvettes with 6 μm polypropylene windows and frozen rapidly in liquid nitrogen. X-ray absorption spectra were measured at the National Synchrotron Light Source (NSLS), beamline X3B, with a Si(111) double-crystal monochromator; harmonic rejection was accomplished using a Ni focusing mirror. Fluorescence excitation spectra for all samples were measured with a 31-element solid-state Ge detector array. Samples were held at approximately 15 K in a Displex cryostat. EXAFS data collection and reduction were performed according to published procedures.[26] Data were measured in duplicate, six scans at the zinc *K*-edge, eight scans at the cobalt *K*-edge, each on two samples from independent purifications; fits to the two data sets were equivalent. As both data sets gave similar results, the data were averaged using EXAFSPAK (EXAFSPAK is available free of charge from http://www-ssrl.slac.stanford.edu/~george/exafspak/exafs.htm); the experimental spectra presented here are the averaged data sets (12−16 scans per sample). The data were converted from energy to *k*-space using E_0 = 9680 eV (Zn) or 7730 eV (Co).

Fourier-filtered EXAFS data were fit using the nonlinear least-squares engine of IFEFFIT, which is distributed with SixPack (SixPack is available free of charge from http://home.comcast.net/~sam_webb/sixpack.html; IFEFFIT is open source software available from http://cars9.uchicago.edu/ifeffit). Theoretical amplitude and phase functions were calculated with FEFF v. 8.00.[27] Zinc-nitrogen single-scattering and zinc-imidazole multiple-scattering was calibrated to the experimental EXAFS of zinc tetrakis-1-methylimidazole Zn(II) perchlorate, $[Zn(MeIm)_4][ClO_4]_2$. Zinc-sulfur scattering was calibrated to the experimental EXAFS of tetrabutylammonium zinc tetramesitylthiolate, $[Bu_4N]_2[Zn(Smes)_4]$. Optimum scale factors (S_c) and ΔE_0 were derived from fits to the model data (S_c = 0.78 (Zn−N) or 0.91 (Zn−S); ΔE_0= −21 eV) and were held fixed at these values for fits to metalloprotein data. The models used for the calibration of cobalt−nitrogen (and cobalt-imidazole) and cobalt−sulfur scattering were, respectively, hexakis-imidazole cobalt(II) perchlorate, $[Co(Im)_6][ClO_4]_2$ and tetrabutylammonium cobalt(II) tetramesitylthiolate, $[Bu_4N]_2[Co(Smes)_4]$, respectively. The resulting S_c and ΔE_0 (S_c = 0.79 (Co−N) or 0.85 (Co−S); ΔE_0 = −21 eV) were held fixed at these calibrated values in subsequent fits to metalloprotein data. First shell fits were then obtained for all reasonable coordination numbers, including mixed nitrogen/oxygen/sulfur ligation, while allowing the absorber-scattered distance, R_{as}, and the Debye−Waller factor, σ_{as}^2, to vary. Detailed summaries of the fitting results are presented in Supporting Information. Multiple scattering contributions from histidine ligands were fitted according to published procedures.[26]

Metal-metal (zinc-cobalt and cobalt-cobalt) scattering were modeled with reference to the experimental EXAFS of Zn_2 (salpn)$_2$ and Co_2 (salpn)$_2$; cobalt-cadmium scattering was fitted empirically, assuming a scale factor of S_c = 1.0.

Stopped-Flow Kinetics. Rapid-scanning visible spectra of chromacef, hydrolyzed by NDM-1, were collected on an Applied Photophysics SX18MV spectrophotometer equipped with a photodiode array detector and a 2 mm path length optical cell. The temperature was kept constant at 9 °C (unless otherwise noted) using a circulating water bath. Absorbance data were converted to concentration as described previously.[19] Stopped-flow fluorescence studies of chromacef hydrolysis were conducted at 9 °C on the same Applied Photophysics spectrometer, using an excitation wavelength of 295 nm and a 320 nm high-pass filter on the photomultiplier. The data obtained in stopped-flow studies were fit with either single or double exponentials using Pro-Data software. Single traces representing substrate, product, or intermediate were simulated with Kinteksim, using the mechanism shown in Scheme 1.

Scheme 1

$$E + S \underset{k_{-1}}{\overset{k_1}{\rightleftharpoons}} ES \underset{k_{-2}}{\overset{k_2}{\rightleftharpoons}} EI \xrightarrow{k_3} E + P$$

EPR Spectroscopy. Low temperature EPR spectra were collected with a Bruker Elexsys E600 EPR spectrometer equipped with an Oxford Instruments ESR900 helium flow cryostat. Spectra were recorded at 9.63 GHz ($B_0 \perp B_1$) or 9.37 GHz ($B_0 \| B_1$) using an ER4116DM dual-mode cavity, with 10 G (1 mT) magnetic field modulation at 100 kHz. Microwave powers and temperatures employed are given in the legends to figures, and other recording parameters were chosen such that resolution was limited by the field modulation amplitude. Spin Hamiltonian parameters were estimated from computer simulations carried out using XSophe (Bruker Biospin), assuming $\hat{H} = \beta gBS + SDS + ASI$, where $S = {}^3/_2$, $D \gg \beta gBS$, and $I(^{59}\mathrm{Co}) = {}^7/_2$, and where $D > 0$ implies $M_S = \pm {}^1/_2$ and $D < 0$ implies $M_S = \pm {}^3/_2$.[28]

Rapid-Freeze-Quench EPR. Variants of NDM-1 (0.5 mM) were reacted with 1.5 mM chromacef, each in buffer at 0 °C. The reaction mixture was rapidly frozen after 10 ms using a previously described system,[29,30] and the quenched samples were analyzed by EPR spectroscopy, as described above. Enzyme−product complex samples were prepared by thawing the quenched reaction samples for 2 min and refreezing.

RESULTS

Generation of apo-, CoCo-, ZnCo-, and CoCd-NDM-1. Previous efforts to prepare metal-substituted forms of NDM-1 involved the initial removal of Zn(II) with EDTA at pH > 7.0; mass spectrometry revealed that the active site cysteine was oxidized under these conditions.[24] We also attempted to prepare apo-NDM-1 by dialyzing the enzyme *vs* EDTA, across a range of pH (6.0−7.5). Metal analyses revealed that the apoenzyme contained < 0.1 equiv of Zn(II), < 0.05 equiv of Fe, and no other common metal ions, regardless of the pH at which it was dialyzed. Direct addition of Co(II) to the apoenzyme resulted in immediate formation of a pink color, which rapidly changed to orange, indicative of Co(II) oxidation.[31] We also attempted a biological incorporation method, developed for preparation of heterodimetallic forms of L1.[21] NDM-1 was overexpressed in minimal medium, and the cell culture was spiked with Co(II) at the time of induction. The resulting enzyme, purified using previously published procedures,[19] contained only 0.6−0.7 equiv of Co and 0.3 equiv of Fe.

Since these more common methods to generate Co(II)-substituted MβLs were unsuccessful with NDM-1, we modified the direct addition method by adding 1 mM TCEP (a reducing agent) to the apoenzyme, prior to adding Co(II). The resulting Co(II)-substituted NDM-1 samples were purple, and this color was retained for months. We generated several other metal-substituted enzymes in this way. Steady-state kinetic studies of all variants, using chromacef as substrate, are summarized in Table 1. All three metal-substituted forms of NDM-1 (ZnCo-, CoCo-, and CoCd-) exhibited steady-state k_{cat} and K_m values within a factor of 3 of those found for ZnZn-NDM-1 (k_{cat} = 4.2 s^{-1}, K_m = 5.1 μM).[19]

Table 1. Steady-State Parameters for Hydrolysis of Chromacef by ZnZn-, ZnCo-, CoCo-, and CoCd- Analogues of NDM-1

species	k_{cat} (s^{-1})	K_m (μM)	k_{cat}/K_m (s^{-1}/μM)	k_{cat}(calc) (s^{-1})[a]	K_m(calc) (μM)[a]
ZnZn	4.2	5.1 ± 0.9	0.8	4.8	0.1
ZnCo	2.0	1.9 ± 0.4	1.0	4.7	0.1
CoCo	3.7	5.6 ± 1.2	0.7	9.4	0.2
CoCd	5.5	5.6 ± 0.7	1.0	14	0.9

[a]Theoretical k_{cat} and K_m calculated using eq 1.

Optical Spectroscopy of Metal-Substituted NDM-1. Previously reported optical spectra for Co(II)-substituted NDM-1 were obtained from samples generated by addition of Co(II) to ZnZn-NDM-1 containing 1 mM EDTA.[19,24] With the new method to generate metal-substituted forms of NDM-1 presented here, we obtained quantifiable optical spectra of ZnCo-, CoCo-, and CoCd-NDM-1 by titration. Addition of Co(II) to apo-NDM-1 suggests that cobalt distributes between the Zn_1 and Zn_2 sites at substoichiometric concentrations (Figure 2A, top), as it does in the B1MβLs BcII,[32,33] Bla2,[34] and IMP-1[35] and as has been shown previously for NDM-1.[24] The ligand field bands between 500 and 650 nm are apparent with as little as 0.25 equiv of added Co(II). At 0.5 equiv of added Co(II), an additional band at 330 nm is observed, and subsequent additions only served to increase the intensity of both features, monotonically. The 330 nm absorption is characteristic of a Cys→Co(II) ligand-to-metal charge transfer, indicative of metal binding at the Zn_2 site, while the structure of the ligand field bands is reminiscent of that exhibited by high-spin Co(II) in the pseudotetrahedral environment of the Zn_1 site.[36] Further addition of Co(II) to this sample resulted in a monotonic increase in absorbance in both regions, maximizing at 2.0 equiv of added Co(II), consistent with binding distributed between the Zn_1 and Zn_2 sites, even at very low concentrations.[22] The final spectra (ε_{330} = 1060, ε_{550} = 505, ε_{615} = 285 M^{-1} cm^{-1} for two Co(II)/protein) are indistinguishable from those reported for many other di-Co(II) B1 MβLs.[18,22,24,32,35,37−40]

The optical spectrum of ZnCo-NDM-1 (Figure 2A, center), prepared by incubation of the apoenzyme with 1 equiv of Zn(II) followed by titration with Co(II), shows a spectrum similar in shape to that obtained from CoCo-NDM-1. Added Co(II) leads directly to the appearance of both the LMCT band at 330 nm and a broad, asymmetric set of ligand field bands (ε_{550} = 220 and ε_{615} = 115 M^{-1} cm^{-1}). However, in this case, maximum absorbance of the LMCT (ε = 900 M^{-1} cm^{-1}) is achieved with 1 equiv of added Co(II), providing strong evidence that it is bound primarily at the consensus Zn_2 site, forming ZnCo-NDM-1.[35] In contrast, when the apoenzyme is incubated with 1 equiv of Cd(II) followed by titration with Co(II), the LMCT at 330 nm is nearly absent. The optical spectrum of CoCd-NDM-1 (Figure 2A, bottom) shows only a nearly symmetric pattern of four principal ligand field bands,

dx.doi.org/10.1021/ja410376s | J. Am. Chem. Soc. 2014, 136, 7273−7285

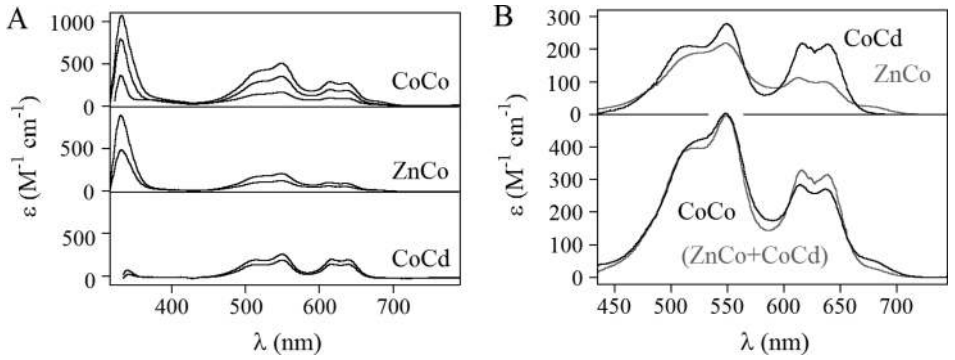

Figure 2. (A) Optical spectra of CoCo-, CoCd-, and ZnCo- analogues of NDM-1. (Top) Titration of apo-NDM-1 with 0.5−2.0 equiv of Co(II). (Center) Apo-NDM-1, incubated with 1 equiv of Zn(II) and then titrated with 0.5 and 1.0 equiv of Co(II). (Bottom) Apo-NDM-1, incubated with 1 equiv of Cd(II) and then titrated with 0.5 and 1.0 equiv of Co(II). The data are plotted on the same scale, offset vertically for clarity. (B) Expanded view of the ligand field region. (Top) Overlay of CoCd- (black) and ZnCo-NDM-1 (gray) spectra. (Bottom) Comparison of the CoCo-NDM-1 ligand field region (black) to the sum of the CoCd- and ZnCo-NDM-1 data (gray).

reminiscent of Co(II)-substituted carbonic anhydrase (CoCA).[41] They maximize at 1 equiv of added Co(II) with ε_{550} = 280 and ε_{615} = 220 M^{-1} cm^{-1}. Thus, the optical spectra are consistent with Co(II) binding at the Zn_1 site in CoCd-NDM-1 and the Zn_2 site in ZnCo-NDM-1.

Closer inspection of the ligand-field regions for ZnCo-NDM-1 and CoCd-NDM-1 (Figure 2B, top) further supports the description of these samples as homogeneous heterobimetallic enzymes. While the CoCd-NDM-1 spectrum is nearly identical to that of resting CoCA,[41] consistent with the pseudotetrahedral geometry anticipated for Co(II) in the Zn_1 site, the ZnCo-NDM-1 spectrum shows a similar pattern of absorption maxima at 510, 550, 615, and 640 nm, along with a shoulder to low energy at 680 nm. However, the intensities are much higher in the higher energy pair, an effect that has been shown to be directly attributable to the thiolate in the coordination sphere of Co(II) in the Zn_2 site.[42] The coordination sphere of the Zn_2 ion most closely resembles that of the active site Zn(II) in farnesyltransferase (FTase),[43] and the ZnCo-NDM-1 spectrum is generally similar to that of Co(II)-FTase,[44] though the four principal features in Figure 2B appear as two unresolved pairs at ∼560 and 635 nm in Co(II)-FTase, with slightly smaller extinction coefficients. Simple addition of the ZnCo- and CoCd-NDM-1 spectra closely matches the ligand field region of the CoCo- enzyme, particularly for the higher energy pair (Figure 2B, bottom). This minimal dependence of the spectrum on the identity of the other metal is consistent with weak coupling between the metals, supported by the EPR (below).

NMR Spectroscopy of Metal-Substituted NDM-1. To better define the binding sites occupied by Co(II) in CoCo-, ZnCo-, and CoCd-NDM-1, ^{1}H NMR spectra were recorded (Figure 3). The NMR spectrum of CoCo-NDM-1 (Figure 3, top) shows a number of hyperfine-shifted signals spanning 170 to −80 ppm. Spectra of similar complexity have been reported for other B1 MβLs, most notably CcrA and BcII,[20,45] with the majority of the resonances upfield of +40 ppm ascribed to secondary interactions with nearby residues in the active site, and those downfield of +40 ppm to ligand protons. Exchange of this sample into D_2O buffer revealed a number of solvent-exchangeable protons (marked by asterisks in Figure 3, both spectra are shown in Supplementary Figure S1). Four of them, clustered between −10 and −25 ppm, presumably arise from outer sphere interactions with backbone amides. The other four (119, 87, 77, and 61 ppm) are readily assigned to the NH protons of Co(II)-coordinated histidines. With analogy to other

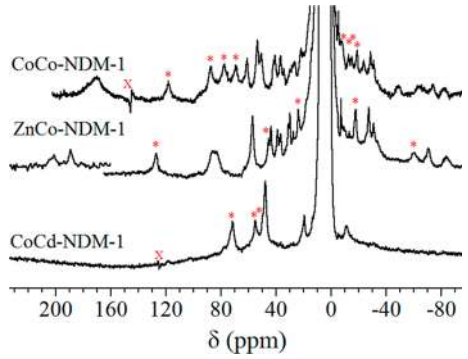

Figure 3. 200 MHz ^{1}H NMR spectra of Co(II)-substituted analogues of NDM-1 in 90% H_2O. Solvent-exchangeable protons are marked with asterisks. Transmitter imperfections are marked with an X.

cobalt-bound cysteinates, we can assign the broad resonance at 170 ppm to one, or both, of the β-CH_2 protons of a Co(II)-coordinated cysteine.[20,25,45−49] The D_2O spectrum (Supplementary Figure S1) reveals a broad resonance at 84 ppm, underlying the two most downfield His resonances. While the chemical shift is consistent with expectation for the α-methylene protons of a terminally Co(II)-coordinated carboxylate,[46,50−52] the similarity of its line width to the resonance at 170 ppm suggests that the resonance at 84 ppm is the geminal partner of the Cys β-proton at 170 ppm. Previous studies of blue-copper proteins have shown that difference in the Cys β-CH_2 proton chemical shifts is directly proportional to the Co−S−C−H dihedral angle.[47,48,53−56] The 86 ppm chemical shift difference, therefore, indicates a significant deviation in the Co−S−C−H dihedral angles from the symmetric ideal of 60°. Of the remaining nonexchangeable resonances (most likely among the three at 50, 53, and 61 ppm), two are likely from the α-CH_2 geminal pair of Asp124.[51]

The NMR spectrum of ZnCo-NDM-1 (Figure 3, center) retains the majority of the weakly and upfield-shifted resonances seen for CoCo-NDM-1. However, it retains only one of the four solvent-exchangeable resonances assigned to His NH protons in CoCo-NDM-1. This resonance most likely derives from His250, which is the only histidine in the Zn_2 site of NDM-1. Its chemical shift increases from 119 to 127 ppm, reflecting loss of the competing influence of a second, likely antiferromagnetically coupled Co(II) ion (below). A similar observation can be made for all of the ligand protons to the

dx.doi.org/10.1021/ja410376s | J. Am. Chem. Soc. 2014, 136, 7273−7285

Zn_2-site: all of their chemical shifts increase when a diamagnetic metal occupies the Zn_1 site. The most downfield shifted Cys β-methylene protons could not be observed, except when the transmitter was placed within ±20 ppm. Under these conditions, two distinct resonances are observed, at 189 and 201 ppm. Assignment of these two resonances as the Cys β-CH_2 geminal pair would require the β-proton chemical shift difference to be reduced from 86 to 12 ppm, on swapping Co(II) for Zn(II) in the Zn_1-site. This can happen only if the Zn_2-site Co(II) ion's **g** tensor reorients *significantly* between the two forms of the enzyme (assuming the cysteine is in the same conformation in both proteins). Alternatively, the observation of two distinct resonances in this region could represent two distinct subpopulations that differ slightly in dihedral angle. We favor this interpretation, as the remainder of the spectrum, in particular the nonexchangeable resonances at 57 and 86 ppm, closely resembles that of CoCo-NDM-1. The broad resonance at 86 ppm also shows evidence of two closely overlapped signals and is similar in width and position to the 84 ppm resonance apparent in the CoCo-NDM-1 spectrum in D_2O (Supplementary Figure S1). The 57 ppm resonance is substantially more intense in the ZnCo-NDM-1 spectrum relative to the analogous resonances in the CoCo-NDM-1 spectrum. We therefore suggest that this resonance most likely arises from the α-CH_2 pair of Asp124, showing a slight alteration of the Co−O−C−H dihedral angle when the metal in the Zn_1-site is changed.

In contrast, the NMR spectrum of CoCd-NDM-1 (Figure 3, bottom) is remarkably simple, with only six prominent hyperfine shifted signals, including a poorly resolved pair at 48−50 ppm. Exchange of this sample into D_2O buffer revealed that three of these are solvent-exchangeable (at 50, 56, and 71 ppm, Supplementary Figure S1). The pattern, together with the optical spectra discussed above, suggests these should be assigned to the NH protons of His120, His122, and His189 in the Zn_1 site. Overall, the chemical shift dispersion displayed by the ligand protons when Co(II) occupies the Zn_1 site (CoCd-NDM-1) is smaller than when Co(II) occupies the Zn_2 site (ZnCo-NDM-1). These observations are consistent with a 5-coordinate Co(II) in ZnCo-NDM-1, expected to display relatively large dipolar shifts, and a 4-coordinate Co(II) in CoCd-NDM-1, which should induce only minimal dipolar shifts.[57−59] The simplicity of the CoCd spectrum further indicates that the majority of the second sphere interactions that give rise to hyperfine shifted proton signals in the CoCo spectrum derive from the Zn_2 site, and their absence further attests to the homogeneity of the Co(II) population in the CoCd enzyme.

EXAFS of Resting CoCo-, ZnCo-, and CoCd-NDM-1. EXAFS spectroscopy was used to further verify the fidelity of the metal substitutions, including the presence of an intact binuclear center, and to probe the metal−metal separations. Fourier-transformed Co *K*-edge EXAFS data for CoCo-NDM-1 are shown at the top of Figure 4. Detailed fitting results for all three metal-substituted variants are presented in Supplementary Figures S2−S4 and Tables S1−S3. Pertinent details are summarized in Table 2. The best fit to the CoCo-NDM-1 data indicated a first shell of 4 N/O and 0.5 S donors per Co. Inclusion of the sulfur in the fit is critical, based on a 47% improvement in the first-shell fit residual (see Supplementary Figure S2 and Table S1, compare fits S1-1 and S1-2). Multiple scattering analyses indicate an average of 2 imidazoles per Co, while the addition of a Co-Co vector at 3.51 Å resulted in a

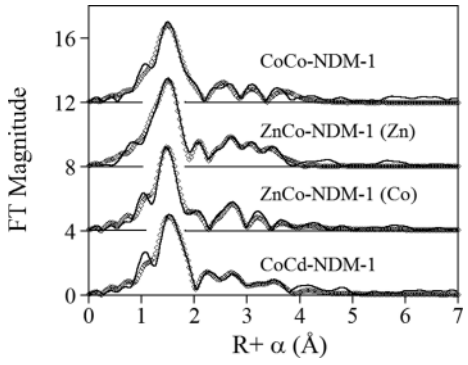

Figure 4. Fourier-transformed EXAFS spectra (solid lines) for metal-substituted forms of NDM-1 and best fits (open symbols). From top to bottom: CoCo-NDM-1 (Co *K*-edge), ZnCo-NDM-1 (Zn *K*-edge), ZnCo-NDM-1 (Co *K*-edge), CoCd-NDM-1 (Co *K*-edge).

66% reduction in the fit residual (compare fits S1-3 and S1-4). This is 0.13 Å longer than the 3.38 Å Zn−Zn separation in ZnZn-NDM-1,[19] reflecting the larger covalent radius of Co(II). The EXAFS clearly show that addition of 2 equiv of Co(II) to apo-NDM-1 results in formation of an intact, singly bridged binuclear center.

XAS of ZnCo-NDM-1 affords the unique opportunity to examine both metal sites independently. The best fits to the Fourier-transformed Zn *K*-edge and Co *K*-edge EXAFS data for ZnCo-NDM-1 are also shown in Figure 4; detailed fitting results are shown in Supplementary Figures S3 and S4 and Tables S2 and S3, respectively. The Zn *K*-edge EXAFS data were best fit with a first shell of 4 N/O donors, including 3 imidazole ligands per Zn(II). Addition of a Co−Zn scattering pathway at 3.45 Å improved the fit residual by 30% (compare fits S2-2 and S2-3). Inspection of the corresponding fits (Supplementary Figure S3) shows that the metal−metal vector dramatically improves the fit at $R + \alpha > 2.8$ Å, but a shorter distance interaction near $R + \alpha \approx 2.1$ Å remains unmatched. We initially attempted to fit this part of the spectrum with a Zn−S interaction, on the assumption that perhaps it represented a small amount of scrambling between the two metal sites, and would thus give us a semiquantitative measure of the homogeneity of the enzyme. However, all attempts to fit this interaction as a Zn−S were visually unsatisfactory, leading to only marginal improvements in the fit residuals and mostly unreasonable distances (compare fits S2-3 and S2-5). The largest Zn−S contribution that gave reasonable parameters would suggest no more than 20% of the total enzyme held Zn(II) in the Zn_2 site. In contrast, inclusion of a Zn−$C_{CO_2}^-$ interaction at 2.51 Å nicely reproduced this feature and reduced the fit residual by a remarkable 73% (compare fits S2-3 and S2-4). The requirement that this feature be a part of the final fit suggests a more intimate connection to Asp124 than expected for metal bound at the Zn_1 site, but the presence of an additional carboxylate bridge would be expected to lead to substantially shorter metal−metal separations than observed.[26,60]

The corresponding Co *K*-edge EXAFS were best fit with a first shell of 4 N/O and 1 S donor (inclusion of the cobalt−sulfur path improves the fit by 46%; compare fits S3-1 and S3-2). Multiple scattering fits indicate only one imidazole ligand, while inclusion of an additional Co−Zn scattering pathway at 3.47 Å improved the fit to the data by 26% (compare fits S3-3 and S3-4). In this case, inclusion of a Co−C_{CO2}^- scattering pathway at 2.47 Å further lowered the fit residual by another 44%. The

dx.doi.org/10.1021/ja410376s | J. Am. Chem. Soc. 2014, 136, 7273−7285

Table 2. EXAFS Fitting Results for Metal-Substituted NDM-1[a]

species	model	M−N/O	M−S	M−M	fit
ZnZn	4 N/O (2 His) + 0.5 S	1.98 (4.5)	2.25 (4.5)	3.38 (7.6)	*b*
CoCo	4 N/O (2 His) + 0.5 S	2.06 (5.3)	2.29 (5.1)	3.51 (6.9)	S1-4
ZnCo (Zn)	4 N/O (3 His)	2.01 (6.5)		3.45 (11)	S2-4
(Co)	4 N/O (1 His) + 1 S	2.03 (4.7)	2.32 (5.1)	3.45 (15)	S3-5
CoCd (Co)	4 N/O (3 His)	2.01 (3.4)		3.56 (13)	S1-3

[a]Distances (Å) and disorder parameters (in parentheses, σ^2 (10^{-3} Å^2)). Fits correspond to those shown in Figure 4; for details, see Supporting Information. [b]Fit S1-4 from ref 19.

two M−M fits are in excellent agreement, and the set show a smooth progression, from 3.38 (Zn−Zn) to 3.45 (CoZn) to 3.51 Å (CoCo). Taken together, the EXAFS of ZnCo-NDM-1 indicate a highly homogeneous enzyme, with Zn(II) binding at the Zn_1 site and Co(II) binding at the Zn_2 site in a heterodimetallic center.

Fourier-transformed Co *K*-edge EXAFS data for CoCd-NDM-1 are shown at the bottom of Figure 4. Detailed fitting results are shown in Supplementary Figure S5 and Table S4. The best fit was obtained with a first shell of 4 N/O donors. The addition of a sulfur scatterer in the first shell resulted in a poorer fit (not shown). Multiple scattering fits indicate 3 imidazole ligands per Co ion. Inclusion of a Co−Cd vector at 3.56 Å improved the fit by about 26%. A second shallow minimum is observed with a 3.79 Å Co−Cd vector, and a fit that includes both distances, refining the respective coordination numbers, suggests no more than an 80/20 distribution between the two distances. Overall, these data are again consistent with the description above, with Co occupying the Zn_1 site and Cd occupying the Zn_2 site in CoCd-NDM-1, in an intact binuclear center.

EPR of Resting CoCo-, ZnCo-, and CoCd-NDM-1. The EPR spectrum of CoCo-NDM-1 under nonsaturating conditions (Figure 5A) exhibited a broad, axial signal with a peak at $g' = 5.2$ (1300 G) that could be simulated assuming an axial **g** tensor with $M_S = \pm {}^1/_2$, $g_\perp = 2.26$, $g_\parallel = 2.45$, and $E/D = 0.1$. All of the $B_0 \perp B_1$ EPR spectra contain a sharp signal at $g' \approx 4.3$ (1800 G) that is due to a few percent of bound Fe(III). The broad lines and the proximity of the Co(II) ions in the Zn_1 and Zn_2 sites suggests spin−spin coupling between the Co(II) ions, and integer-spin signals were directly observable at lower temperature and higher power (Figure 5B) and with $B_0 \| B_1$ (Figure 6A). A resonance at $g' \approx 8$ (800 G) suggested a transition in the $S' = 2$ manifold of an $S = 0, 1, 2, 3$ spin ladder, and a distinct signal appearing out of zero field is indicative of interdoublet transitions. These signals require the value of J to be very small, on the order of a few cm^{-1} or less, consistent with the optical spectra. A trough in the high power/low temperature spectrum (Figure 5B) at $g' \approx 3.1$ (2170 G) is due to rapid passage of the slow-relaxing axial species at the lower temperature and higher power compared to the spectrum in Figure 5A.

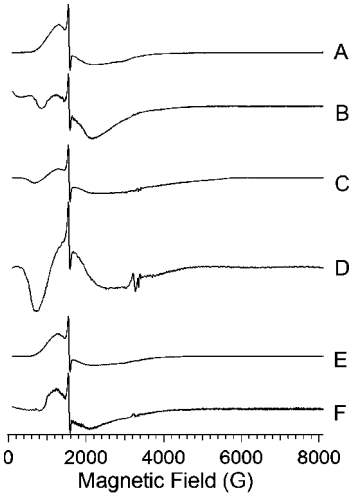

Figure 5. Perpendicular mode RFQ-EPR spectra of the reaction of CoCo-NDM-1 with chromacef. Spectra A and B are from resting CoCo-NDM-1. Spectra C and D are from CoCo-NDM-1 after reaction with chromacef for 10 ms at 3 °C. Spectra E and F are from CoCo-NDM-1 after incubation with chromacef for 2 min (at which time all of the added chromacef has been hydrolyzed). Spectra A, C, and E were recorded at 10 K and 1 mW, and spectra B, D, and F were recorded at 5 K, 63 mW. Spectral intensities were adjusted for (i) $1/T$, (ii) $\sqrt{}$(microwave power), and (iii) dilution during rapid-freeze quenching. In addition, spectra A, C, and E are shown multiplied by a factor of 2 relative to B, D, and E.

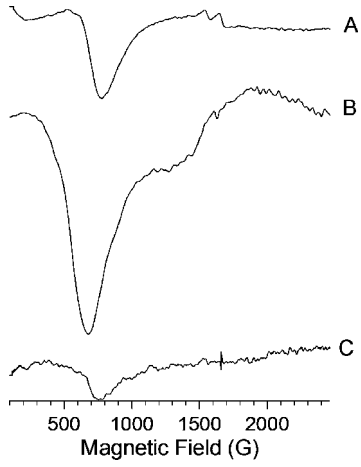

Figure 6. Parallel mode RFQ-EPR spectra of the reaction of CoCo-NDM-1 with chromacef. Spectrum A is from resting CoCo-NDM-1. Spectrum B is from CoCo-NDM-1 after reaction with chromacef for 10 ms at 3 °C. Spectrum C is from CoCo-NDM-1 after incubation with chromacef for 2 min. All spectra were recorded at 5 K and 63 mW and are shown with the correct relative intensities.

The EPR spectrum of ZnCo-NDM-1 (Figure 7A and inset) is complex and appears to contain at least three species. The major contribution is from a rhombic species characterized by a ^{59}Co hyperfine pattern centered at $g' \approx 6.65$ (1010 G), of which only the higher field lines are well-resolved due to correlated strains in g and A, and broad resonances at ∼ 2800 and ∼ 4000 G. Simulations showed that this signal could not be modeled assuming an axial **g** tensor and, therefore, that no unique solution exists in terms of spin Hamiltonian parameters. This species was readily simulated assuming a nonunique

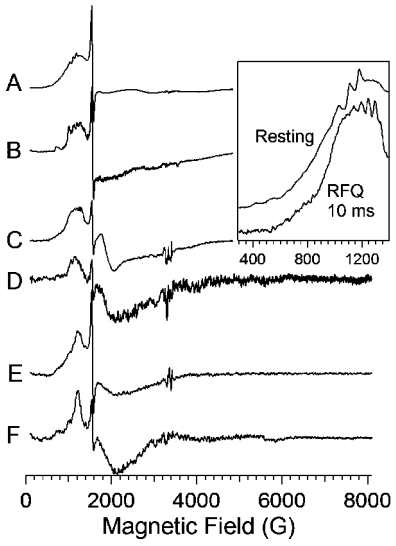

Figure 7. Perpendicular mode RFQ-EPR spectra of the reaction of ZnCo-NDM-1 with chromacef. Spectra A and B are from resting ZnCo-NDM-1. Spectra C and D are from ZnCo-NDM-1 after reaction with chromacef for 10 ms at 3 °C. Spectra E and F are from ZnCo-NDM-1 after incubation with chromacef for 2 min. Spectra A, C, and E were recorded at 10 K and 1 mW, and spectra B, D, and F were recorded at 5 K, 63 mW. Spectral intensities were adjusted for (i) $1/T$, (ii) $\sqrt{}$(microwave power), and (iii) dilution during rapid-freezing. In addition, further multiplication factors were applied to spectra B (×0.5), D (×0.5), E (×3), and F (×0.5). The inset shows expanded views of A ("Resting") and C ("RFQ 10 ms") that highlight the ^{59}Co hyperfine splitting.

rhombic **g** tensor, and further, it could be simulated assuming either $M_S = \pm {}^1/_2$ (*e. g.*, with $g_{x,y,z}$ = 2.45, 2.70, 2.25; E/D = 0.32; $A(^{59}\text{Co}) = 9.0 \times 10^{-3}$ cm^{-1}) or $M_S = \pm {}^3/_2$ (*e. g.*, with $g_{x,y,z}$ = 2.38, 2.60, 2.67; E/D = 0.32; $A_y(^{59}\text{Co}) = 9.0 \times 10^{-3}$ cm^{-1}). The inability to distinguish $M_S = \pm {}^1/_2$ and $M_S = \pm {}^3/_2$ prevents an assignment of coordination number, though the high value of E/D and the relatively slow relaxation of the signal suggests that 5-fold coordination is more likely than 4-fold, and both are much more likely than 6-fold. There is a broad axial feature underlying the rhombic signal, which is likely due to a small amount of unbound Co(II) or to a subpopulation of CoCo-NDM-1 in the nominally ZnCo-NDM-1 sample.

At lower temperature (Figure 7B) there is evidence, in the form of an additional peak at g' = 6.65 (1010 G), for a third signal consistent with a distorted tetrahedral species. While this signal is small and in this case represents a minor contributor, it should be appreciated that the g'_x and g'_y values may be very low (approaching zero for true octahedral coordination), and that the g'_x and g'_y resonances may therefore be at very high field, making quantitation difficult. The peak intensity of an EPR signal is inversely related to the square of the spectral field envelope width and the peak intensity of an $S = {}^3/_2$, $M_S = \pm {}^3/_2$ EPR signal due to a nominally tetrahedrally coordinated Co(II) ion would be expected to be small compared to also-present $M_S = \pm {}^1/_2$ signals, even if it accounted for a considerable fraction of the spins. The present signal may arise from a small subpopulation of CoZn-NDM-1 (with Co(II) in the Zn_1 site) or, alternatively, a subpopulation of four-coordinate Co(II) in the Zn_2 site. Another resonance is visible in the spectrum of ZnCo-NDM-1 at 5 K, a feature that peaks at about g' = 9.6 (700 G). The line shape of this resonance and the fact that the EPR absorption ends abruptly at g' = 10.0 suggest that it is due to transitions in either or both of the $M_S = \pm {}^1/_2$ and $\pm {}^5/_2$ doublets of $S = {}^5/_2$ Fe(III) with high strains in E and that it is related to the line at g' = 4.3.[61]

The EPR spectrum of CoCd-NDM-1 (Figure 8A) exhibited an axial signal with a peak at g' = 5.25 (1280 G) and a resolved

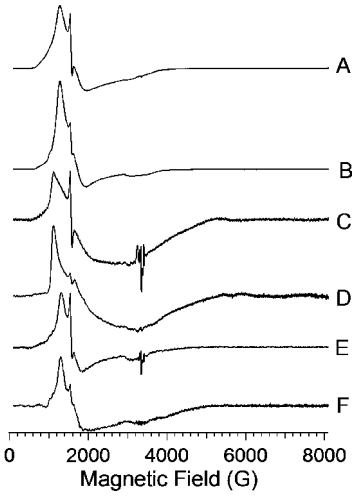

Figure 8. Perpendicular RFQ-EPR spectra of the reaction of CoCd-NDM-1 with chromacef. Spectra A and B are from resting CoCd-NDM-1. Spectra C and D are from CoCd NDM-1 after reaction with chromacef for 10 ms at 3 °C. Spectra E and F are from CoCd NDM-1 after incubation with chromacef for 2 min. Spectra A, C, and E were recorded at 10 K and 1 mW, and spectra B, D, and F were recorded at 5 K, 63 mW. Spectral intensities were adjusted for (i) $1/T$, (ii) $\sqrt{}$(microwave power), and (iii) dilution during rapid-freeze quenching. In addition, further multiplication factors were applied to spectra B (×0.17), C (×4), E (×4), and F (×0.5).

g_z resonance at about 2400 G. Simulations returned the parameters $M_S = \pm {}^1/_2$, $g_\perp$ = 2.32, $g_\parallel$ = 2.40, and E/D = 0.09, which are most consistent with 5- or 6-fold coordination. Although the assignment to 5-fold coordination is supported by the resistance of the signal to rapid passage effects at 5 K (Figure 8B), the relatively narrow $g_\perp$ feature argues against the two coordinated water molecules that would be required. The reduced *g*-anisotropy relative to the CoCo enzyme and clearly axial symmetry of the CoCd EPR are consistent with the more centrosymmetric environment of the pseudotetrahedral Zn_1 site.[62,63] The very different respective values for E/D strongly differentiate the predominant Co(II) species in ZnCo-NDM-1 and in CoCd-NDM-1 and indicate that the axial electronic symmetry and, by inference, the ligand field symmetry are much higher in the Zn_1 site than in the Zn_2 site. This perhaps is to be expected given the lone cysteine residue in the Zn_2 site and the intense charge-transfer transition in the optical spectrum of Co(II) in the Zn_2 site (Figure 2).

Simulations and comparison of the spectra of CoCd-NDM-1 at 5 and 10 K (Figure 8A, B) indicate an underlying broad signal at 10 K that contributes a broad shoulder to low field of the main peak and absorption at 2000−4000 G that obscures the g_z feature of the axial species that is well-resolved at 5 K. This broad feature is likely due to unbound Co(II), which at 5 K and 63 mW is broadened beyond detection. A small additional EPR signal was observed at 5 K, apparent as a step on the low-field side of the main peak at $g' \approx 6.35$ (1035 G) and is tentatively assigned to a minor contribution from a second distorted tetrahedral species.

Diode-Array Optical Studies of ZnZn-, CoCo-, ZnCo-, and CoCd-NDM-1. Previously, we used diode-array optical

dx.doi.org/10.1021/ja410376s | J. Am. Chem. Soc. 2014, 136, 7273−7285

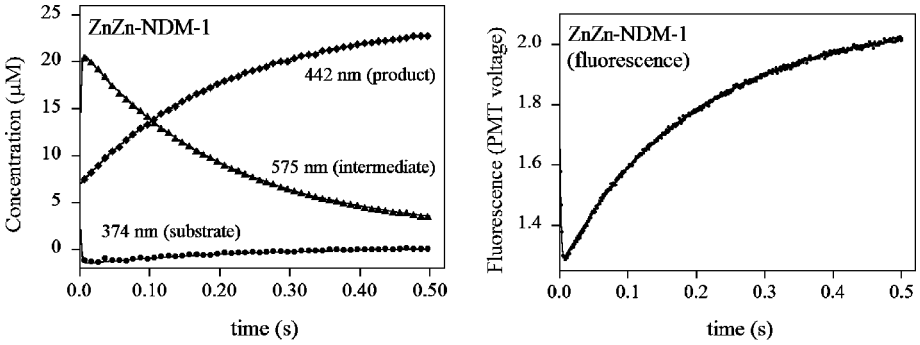

Figure 9. Progress curves for reaction of 22.5 μM chromacef with 25 μM ZnZn-NDM-1 at 9 °C, under single turnover conditions. (A) Reaction followed by diode array spectrophotometry. (B) Reaction followed by tryptophan fluorescence emission. In both, the symbols are experimental data (only 1/10th of the data points are shown, for clarity), and the solid lines are Kinteksim simulations, based on the mechanism in Scheme 1.

studies at 9 °C to probe the pre-steady-state reaction of NDM-1 with chromacef, and we utilized kinetic simulations to offer a minimal kinetic scheme for the enzyme.[19] These studies revealed that the hydrolysis of chromacef by ZnZn-NDM-1 proceeds through an anionic nitrogen intermediate, and the decay of this intermediate is rate-limiting for NDM-1 when chromacef or nitrocefin are used as substrate. Here, the reaction of 25 μM ZnZn-NDM-1 with 22.5 μM chromacef was monitored using an Applied Photophysics diode array spectrophotometer, and progress curves corresponding to substrate decay (374 nm), intermediate formation/decay (575 nm), and product formation (442 nm) were generated (Figure 9A). Under these conditions, a large amount of the reaction intermediate is formed over the first 10 ms of the reaction, and the rate of intermediate decay (4.8 s^{-1}) is identical to the rate of product formation (4.9 s^{-1}) (Table 3). The rate of substrate decay (505 s^{-1}) is also very similar to the rate of intermediate formation (582 s^{-1}).

Reaction of the metal-substituted variants of NDM-1 with chromacef was examined in the same way. The rates of substrate decay, intermediate formation/decay, and product formation, obtained from single or double exponential fits, are shown in Table 3. The corresponding progress curves are shown in Supplementary Figure S6. In all cases, a significant amount of the intermediate was formed, and its rate of formation mirrored the rate of substrate decay. Interestingly, the rate of intermediate formation is reduced almost 2-fold when Zn(II) is replaced with Co(II) in the Zn_2 site, while the rate of product formation is unaffected. The rate of intermediate formation is reduced further, by another factor of 2, when both Zn(II) ions are replaced with Co(II), while conversion to product doubles for the CoCo enzyme. Similarly, the CoCd enzyme forms the intermediate ca. 2-fold more slowly than its CoCo analogue and nearly 10-fold more slowly than the ZnZn enzyme, while it converts the intermediate to product 3-fold more quickly. In total, the data offer a clear indication that the acidity of the metal ion in the Zn_2 site is critical to stabilization of the anionic intermediate and further demonstrate a role for each metal ion in both intermediate formation and its conversion to product. Most importantly, the data show that all three metal-substituted forms use the same minimal mechanism as ZnZn-NDM-1.

Microscopic rate constants were determined by fitting the progress curves to the mechanism in Scheme 1, using Kinteksim. The mechanism in Scheme 1 differs from that used in our preceding study, in that it lacks the formation of a product-complex, as indicated by the RFQ-EPR studies described below. The resulting simulated traces match the experimental data very well (Figure 9A and Supplementary Figure S6). Results of the fits are summarized in Table 3. The microscopic rates for substrate decay, intermediate formation/decay, and product formation from Table 3 were used to calculate theoretical k_{cat} and K_m values according to eq 1, and these values are included, for comparison to the steady-state values, in Table 1. The calculated values differ substantially (20- to 50-fold) for K_m, less so (2- to 3-fold) for k_{cat}. This disparity arises from inclusion of the substrate on/off rates (k_1/k_{-1}) in K_m. Without an experimental measure, the on rate (k_1) was held fixed at the diffusion limit, while the off rate (k_{-1}) was treated as a parameter.

$$k_{cat} = \frac{k_2 k_3}{k_2 + k_3} K_m = \frac{k_3(k_{-1} + k_2)}{k_1(k_2 + k_3)} \quad (1)$$

Included in Table 3 is a reanalysis of our earlier results for the reaction of ZnZn-NDM-1 with chromacef, obtained at

Table 3. Results of Single Turnover Experiments with Chromacef at 9 °C

species	measurement	k_2 (s^{-1})	k_3 (s^{-1})[a]
ZnZn	fluorescence	676 ± 11	5.1
	A_{374}	505 ± 19	
	A_{442}		4.8
	A_{575}	582 ± 7	4.9
	sim (9 °C)[b]	670 ± 70	4.8
	sim (15 °C)[b]	395 ± 7	8.7
	sim (22 °C)[c]	700 ± 100	12.0
ZnCo	fluorescence	225 ± 6	3.7
	A_{374}	290 ± 8	
	A_{442}		4.5
	A_{575}	341 ± 4	4.5
	sim[b]	550 ± 50	4.7
CoCo	fluorescence	135 ± 2	10.4
	A_{374}	156 ± 5	
	A_{442}		10.1
	A_{575}	183 ± 3	10.1
	sim[b]	500 ± 50	10.0
CoCd	fluorescence	65 ± 1	15.7
	A_{374}	54 ± 1	
	A_{442}		15.5
	A_{575}	77 ± 1	14.8
	sim[b]	150 ± 70	16.0

[a]Uncertainty in k_3 is ca. ± 0.1. [b]From Kinteksim simulations, using the mechanism in Scheme 1. The value of k_1 was held fixed at 10^9 s^{-1}. Values of k_{-1} ranged from 4000 to 8000 (±1000). [c]From a reanalysis of the data reported in ref 19, using the mechanism in Scheme 1.

dx.doi.org/10.1021/ja410376s | J. Am. Chem. Soc. 2014, 136, 7273−7285

22 °C (rather than the 9 °C used broadly here), along with an additional measurement at 15 °C. Perhaps not surprisingly, the only microscopic rate constant affected by temperature is the rate-limiting step, k_3, which increases 2.5-fold from 9° to 22 °C. This suggests a large energy of activation associated with product release, and an Arrhenius plot involving k_3 (Supplementary Figure S7) sets the energy of activation at 12 ± 2 kcal mol^{-1}, in good agreement with values obtained through QM/MM calculations on CcrA (B1)[64] and L1 (B3).[65] The associated Eyring plot (Supplementary Figure S7) shows a large entropic contribution to the energetics of product generation ($\Delta H^{\ddagger}$ = 5.2 kcal mol^{-1}; $\Delta S^{\ddagger}$ = 8.4 kcal mol^{-1} K^{-1}.

Stopped-Flow Fluorescence of ZnZn-, ZnCo-, CoCo-, and CoCd-NDM-1. The crystal structure of resting ZnZn-NDM-1 shows that Trp93 is ca. 8.0 and 5.7 Å from the metal ions in the Zn_1 and Zn_2 binding sites, respectively.[66] These distances increase to 8.1−8.4 Å (Zn_1) and 6.0−6.2 Å (Zn_2) in the structure of hydrolyzed meropenem bound to ZnZn-NDM-1. Similar distance increases with bound hydrolyzed ampicillin, benzylpenicillin, methicillin, oxacillin, and captopril have been observed,[67,68] suggesting the fluorescence of Trp93 can be used to monitor the reaction with substrate, as was demonstrated previously with MβL L1 and nitrocefin.[69,70]

Stopped-flow fluorescence studies at 9 °C using 25 μM ZnZn-NDM-1 and 22.5 μM chromacef revealed a biphasic curve in which the fluorescence dropped precipitously during the first 10 ms of the reaction and then increased exponentially over the next 500 ms (Figure 9B). These data are similar to those reported for L1 with nitrocefin, and fitting these data to a double-exponential yielded rate constants of 676 s^{-1} for the fluorescence decay and 5.1 s^{-1} for the fluorescence return (Table 3). These values are very similar to those obtained from the diode array studies. Control experiments using apo-NDM-1 showed no changes in fluorescence, demonstrating the observed signal changes were due to substrate binding/catalysis. CoCo-, ZnCo-, and CoCd-NDM-1 each exhibited fluorescence progress curves similar to that of ZnZn-NDM-1 (Supplementary Figure S6). The rates of fluorescence decay/return (s^{-1}) were 134/10.3, 225/4.6, and 65/15.7 for CoCo-, ZnCo-, and CoCd-NDM-1, respectively.

Since the rates of fluorescence growth were very similar to the rates of product formation in the single-turnover diode array studies, we used the fluorescence quenching rates as a function of chromacef concentration to determine K_s values for substrate binding to the various isoforms.[71] A representative plot is shown in Figure 10. The K_s values, determined by fitting these data to eq 2, for ZnZn-, ZnCo-, CoCo-, and CoCd-NDM-1 were 14.6, 18.1, 12.3, and 11.2 μM, respectively. These values clearly suggest that metal substitution does not significantly alter substrate affinity.

$$k_{obs} = \frac{k_f[S]}{K_s + [S]} + k_r \qquad (2)$$

RFQ-EPR of CoCo-, ZnCo-, and CoCd-NDM-1. To gauge the intimate changes taking place at each metal site, we performed rapid-freeze-quench EPR experiments. For each of the CoCo-, ZnCo-, and CoCd-NDM-1 species, quite dramatic effects were observed in the EPR spectra upon reaction with chromacef. These effects were distinct for each of the species, providing insight into the role of each metal ion and the metal center as a whole.

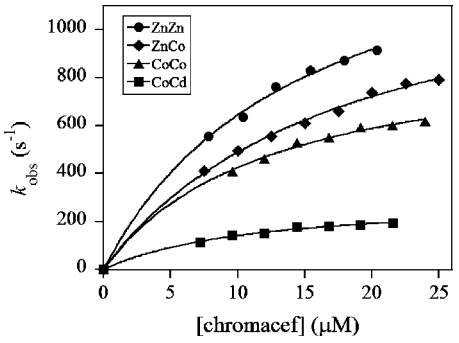

Figure 10. Plot of observed rate constant for fluorescence emission quenching (k_{obs}, s^{-1}) versus chromacef concentration for ZnZn-, ZnCo-, CoCo-, and CoCd-NDM-1. K_s was determined by fitting the data to eq 2 for each analogue.

In CoCo-NDM-1, about two-thirds of the g' = 5.2, $S = {}^3/_2$, $M_S = \pm {}^1/_2$ signal is lost upon reaction with chromacef for 10 ms at 3 °C (Figure 5). The zero-field signal is lost completely, and a new integer-spin signal with g' = 9.2 (725 G) is observed with about three times the intensity of the g' = 8 signal from the resting enzyme. In parallel mode, where the g' values are consistently larger than those observed when $B_0 \perp B_1$, the shift upon reaction with chromacef is from g' = 8.6 to g' = 9.9 (Figure 6). This may indicate a shift from S' = 2, which is an excited state of the spin ladder and indicates antiferromagnetic coupling in the absence of a ground state accompanying S' = 3 signal, to an S' = 3 ground state of a ferromagnetic spin ladder (S' = 3, 2, 1, 0). Such signals have been found for phosphonate-bridged Co(II) ions in the active site of aminopeptidase from *V. proteolyticus*.[72] By analogy, then, we tentatively assign the signal to bidentate binding of chromacef across the two Co(II) ions in CoCo-NDM-1, suggesting a rationale for the dinuclear metal center in NDM-1. Upon completion of the reaction, only a very weak residual integer-spin signal was observed, and only with $B_0 \| B_1$ (Figure 6C). Although the integer-spin signal is smaller, measurements with $B_0 \perp B_1$ (Figure 5E, F) show a $S = {}^3/_2$, $M_S = \pm {}^1/_2$ signal that is essentially indistinguishable from the resting signal, indicating that CoCo-NDM-1 does not form a strong product complex.

The most striking change in the EPR spectrum of ZnCo-NDM-1 upon reaction with chromacef (Figure 7) is a change in the ^{59}Co hyperfine splitting, from a typical value of 9 × 10^{-3} cm^{-1} in the resting enzyme to 5.5 × 10^{-3} cm^{-1} (Figure 7C and inset). This indicates significant electron delocalization away from the Co(II), which in turn is indicative of direct and likely multidentate binding of chromacef to Co(II) in the Zn_2 site of ZnCo-NDM-1. The hyperfine-exhibiting species could be simulated and assigned to an $M_S = \pm {}^1/_2$ ground state with moderate rhombic distortion of the axial zero-field splitting, indicating 5-fold geometry ($g_\perp$ = 2.45, $g_\|$ = 2.20, $A_y(^{59}\text{Co})$ = 5.5 × 10^{-3} cm^{-1}, and E/D = 0.17). Upon allowing the reaction to go to completion, a new relatively sharp signal devoid of resolved hyperfine structure was observed at g' = 5.45 (1230 G) (Figure 7E). This signal could be simulated assuming $M_S = \pm {}^1/_2$, $g_\perp$ = 2.32, $g_\|$ = 2.50, and E/D = 0.12, but most of the EPR absorption is featureless, and the signal displayed unusual and anisotropic dependence on temperature and microwave power (Figure 7F) that suggests that more than one species may be involved. The resemblance of the rapid-passage feature at 2000 G in spectrum **7F** to those in **6B** and **6F** suggest either some scrambling of the metal ions upon extended reaction, to form a

dx.doi.org/10.1021/ja410376s | J. Am. Chem. Soc. 2014, 136, 7273−7285

Scheme 2

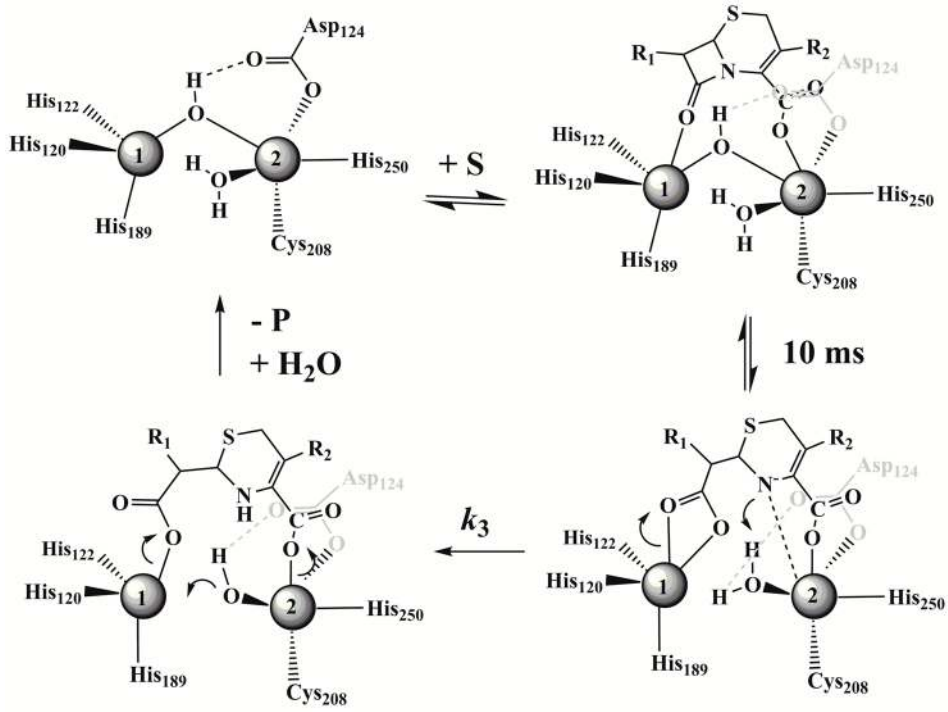

subpopulation of CoCo-NDM-1, or some unbound Co(II) in both the ZnCo- and CoCo-NDM-1 samples.

The EPR spectrum of CoCd-NDM-1 upon reaction with chromacef for 10 ms (Figure 8) showed a quite dramatic shift in the position of the main resonance peak from $g' = 5.25$ (1280 G) to 6.0 (1110 G) (Figure 8C). The peak at $g' = 6.0$ sharpened and increased in intensity by a factor of 4, after applying correction factors, upon lowering the temperature from 10 to 5 K and increasing the power from 1 to 63 mW, indicating very fast relaxation. It is tempting to assign this signal to $M_S = \pm {}^3/_2$, but the broad absorption extending from 2000 to 4000 G exhibited a similar intensity dependence and appeared to begin to resolve into two distinct resonances at the lower temperature, a derivative shape around 1900 G and a g_z absorption line at 3000 G. If all of these resonances are indeed associated, as the relaxation behavior seems to indicate, then the assignment is to a five-coordinate Co(II) with a distorted and highly rigid coordination sphere, providing unusually strong coupling to the lattice. The lack of resolved hyperfine coupling on the $g' = 6$ line (strictly speaking, the g_y resonance of a $S = {}^3/_2$, $M_S = \pm {}^1/_2$ system) means that the coupling is primarily in one of the other orientations and is strain-broadened beyond detection. However, this clearly differentiates the Co(II) in the Zn_1 site of CoCd-NDM-1 from that in the Zn_2 site of ZnCo-NDM-1. Upon extended reaction with chromacef, the EPR signal reverts essentially to the resting state, although the underlying broad absorption in spectrum **8A** is no longer present in spectrum **8E**, indicating that the broad absorption in the resting state is due to a species that is returned to the native state through turnover.

DISCUSSION

The *NDM-1* plasmid that harbors the gene for metallo-β-lactamase NDM-1, along with other resistance genes, has emerged as one of the most important players in recent clinical reports of antibiotic resistance. A great deal of enzymological data has been reported on NDM-1.[19,24,66,67,73−83] To date, structural studies on this enzyme have been limited to X-ray crystallography[66,67] and EXAFS spectroscopy.[19] Successful preparation of spectroscopically active, metal-substituted forms of NDM-1 has allowed us to perform more detailed structural studies, including the use of rapid-freeze-quench methods to examine the catalytic mechanism at the atomic level.

Several different strategies have been developed to prepare metal-substituted forms of the metallo-β-lactamases.[18,21−23,45,84] Previous reports have shown oxidation of the active site cysteine in other B1 MβLs as a direct result of cobalt substitution, most notably for CcrA[45] and BcII.[22] We find that Cys208 in NDM-1 is much more susceptible to Co-mediated oxidation, obtaining only Co(III)-containing and substoichiometrically loaded protein, on direct addition of Co(II) to the apoprotein. The prophylactic addition of a reducing agent (TCEP), prior to addition of Co(II), prevents Co(II)-mediated oxidation, allowing relatively easy preparation of a di-Co(II) form of NDM-1, as well as the heterodimetallic forms reported here. Methods have been described to prepare heterodimetallic forms of other dinuclear zinc enzymes,[85] including the MβLs BcII[20] and L1.[21] However, to our knowledge, this is the first report of metal-substituted MβLs that were site-specifically loaded with a paramagnetic Co(II) ion in *either* the Zn_1 *or* the Zn_2 position, while incorporating a diamagnetic metal ion in the other.

The optical, NMR, EPR, and EXAFS studies presented here clearly support the descriptions above, with an intact dinuclear center in each metal-substituted form, in which the metal ions are sequentially loaded. In combining the results of multiple techniques, it is important to be mindful of the relative sensitivities and limitations of each technique. For example, the optical and NMR studies, as well as the kinetic studies discussed below, were carried out near room temperature, in fluid solution. The optical spectra, with bands spanning

dx.doi.org/10.1021/ja410376s | J. Am. Chem. Soc. 2014, 136, 7273−7285

hundreds of cm^{-1}, will report only gross structural heterogeneity, with subtleties absorbed into the apparent extinction coefficients. NMR is much more sensitive, but only static structural heterogeneity will be easily detected, with dynamic processes manifest as additional broadening of an already broad resonance. In contrast, the EXAFS and the EPR are performed in frozen solution, at or near liquid helium temperatures. EXAFS, as a bulk sampling technique (measuring a weighted average), can tolerate 5−10% of an impurity before it significantly affects the best-fit model, depending on the system. Meanwhile, the EPR is sensitive to the same structural heterogeneity that may appear as line broadening in the NMR, but without dynamics, these are represented as alternate conformations and subpopulations, each with its own EPR response. As the EPR signals of high-spin Co(II) centers span several thousand Gauss at X-band, small changes in electronic structure are readily observed, while the EPR response of Co(II) in a given geometry and the electronic structure associated with it are not easily comparable to the response of Co(II) in another geometry, as described above. Consequently, although the EPR is most sensitive to structural heterogeneity, quantification is difficult. Given these limitations, we can conservatively state that all of the heterobimetallic enzymes studied here were > 90% in the resting form shown in the upper left of Scheme 2, with the metals distributed as indicated.

The EXAFS-derived metal−metal separations (Table 2) track with the covalent radii of the metal ions (3.38 Å (Zn−Zn) to 3.45 Å (Zn−Co) to 3.51 Å (Co−Co) to 3.56 Å (Co−Cd)), suggesting there is only minimal modulation of the metal−oxygen−metal angles, which we would expect to translate into only minor differences in reaction rates, as is seen. In steady-state kinetic studies, all three forms (CoCo-, ZnCo-, and CoCd-NDM-1) were seen to exhibit K_m and k_{cat} values within a factor of 2−3 of those for ZnZn-NDM-1. A similar observation can be made with regard to the single turnover experiments. Stopped-flow fluorescence using chromacef as substrate indicated nearly identical substrate affinities and product release rates within a factor of 3−4 across the series of enzymes, suggesting the metal substitutions did not cause gross changes in the structure of the active site or its ability to function as an MβL.

Stopped-flow optical studies demonstrated that a ring-opened, anionic intermediate was observed with all four metal-substituted forms of NDM-1. While the ZnZn, ZnCo, and CoCo analogues formed the intermediate in near stoichiometric amounts, the CoCd enzyme builds up to only ca. 50% of the total enzyme concentration, the combined effect of a 10-fold decrease in the rate of intermediate formation (k_2 in Table 3) and a 3-fold increase in the rate of product release (k_3), relative to ZnZn-NDM-1. Overall, the rates of intermediate formation and decay are comparable, suggesting that the identity of the metal ions does not greatly affect the overall energetics of the reaction. The rate-limiting step for all four forms of the enzyme is clearly protonation of the intermediate, as proposed earlier for other MβLs.[21,86−88] The product release rates nicely track the Lewis acidity of the metal in the Zn_2 site (Zn(II) > Co(II) > Cd(II)) but are also affected by the identity of the metal in the Zn_1 site. Both forms with Zn(II) in the Zn_1 site (ZnZn and ZnCo) show $k_3 \approx 5\ s^{-1}$ at 9 °C, while the two forms with Co(II) in the Zn_1 site (CoCo and CoCd) are 2−3 times faster at 10 and 16 s^{-1}, respectively. Further freeze-quench spectroscopic studies will be required to completely disentangle the individual contributions.

Rapid-freeze-quench EPR studies showed significant changes in the Co(II) ion electronic structure, whether residing in the Zn_1 site or the Zn_2 site, as well as in the dinuclear Co(II) center, on a catalytically relevant time scale. These observations are summarized in the proposed mechanism in Scheme 2. Co(II) in the Zn_1 site (as in CoCd-NDM-1) undergoes a marked change in electronic structure upon reaction with substrate, indicative of a decrease in coordination symmetry, and exhibits very fast electronic relaxation, suggestive of a very rigid coordination sphere. On the basis of these observations, we favor a five-coordinate Co(II). While Scheme 2 depicts simultaneous coordination of both O atoms from the newly formed carboxylate of the ring-opened intermediate (one from the μ-OH ligand, one from the substrate carbonyl), we cannot rule out the presence of an incoming water molecule, possibly reforming the bridge, and monodentate coordination of the newly formed carboxylate. Either interpretation suggests a clear role for the Zn_1 ion in nucleophile activation and/or delivery.

In contrast, for Co(II) in the Zn_2 site, a dramatic reduction in the ^{59}Co hyperfine splitting provides clear evidence for binding of a moiety capable of absorbing delocalized spin density from the Zn_2-site metal ion, on the same time scale as the events described above for the Zn_1-site metal ion. Only Cd(II) substitution had a significant effect on the rate of intermediate formation, suggesting a major role for the Zn_2 ion in electrophilic activation of the substrate and stabilization of the anionic intermediate, providing further rationale for the coordinated cysteine in the Zn_2 site.[42] We note here that the cysteinate is *trans* to the position the anionic nitrogen would occupy.

The simultaneous binding of the intermediate to both metal ions and the loss of the μ-OH bridge are supported by the RFQ-EPR of CoCo-NDM-1. The resting state spectrum shows that a small proportion of the dinuclear center exists in a very weakly, and probably antiferromagnetically, exchange coupled state. In the 10 ms RFQ sample, on the other hand, more than 60% of the centers exhibit exchange coupling, also weak, but probably ferromagnetic and not due to a commonly bound single atom. After extended reaction, the Zn_1 ion returns to its resting coordination, whereas the electron-density-donating Zn_2 ion remains bound to the product at the high concentrations used for RFQ-EPR. These data are consistent with the very small integer spin signal seen upon extended reaction of CoCo-NDM-1 with chromacef.

■ SUMMARY

In summary, the reaction mechanism of NDM-1 was investigated by creating heterodimetallic forms of NDM-1 and using the chromogenic substrate chromacef. The coordination environment of each metal site was studied by specifically incorporating a paramagnetic Co(II) ion independently into either the Zn_1 or the Zn_2 site. Our kinetic studies demonstrate that the rate-limiting step in the hydrolysis reaction is the decay of a common reaction intermediate, and that the rate of product formation is dependent on the acidity of the metal ion in the Zn_2 site. The spectroscopic studies show clear roles for both metals at all stages of the reaction.

■ ASSOCIATED CONTENT

Ⓢ Supporting Information

Seven figures and four tables showing ^{1}H NMR of CoCo-, ZnCo-, and CoCd-NDM-1 in H_2O/D_2O (Figure S1), detailed EXAFS fitting results for all three (Figures S2−S5 and Tables

S1−S4), diode array and stopped-flow fluorescence progress curves (Figure S6), and Arrhenius and Eyring plots from temperature-dependent kinetics (Figure S7). This material is available free of charge via the Internet at http://pubs.acs.org.

AUTHOR INFORMATION

Corresponding Author

tiernedl@miamioh.edu

Notes

The authors declare no competing financial interest.

ACKNOWLEDGMENTS

This work was supported by the National Institutes of Health (GM093987 to M.W.C. and D.L.T.; EB001980 to B.B.; P30-EB-009998 to the Center for Synchrotron Biosciences from the NIBIB, which supports beamline X3B at the NSLS); and the National Science Foundation (CHE-1151658 to M.W.C. and D.L.T.; CHE-1152755 to D.L.T.).

REFERENCES

(1) Drawz, S. M.; Bonomo, R. A. *Clin. Microbiol. Rev.* **2010**, *23*, 160−201.

(2) Fisher, J. F.; Meroueh, S. O.; Mobashery, S. *Chem. Rev.* **2005**, *105*, 395−424.

(3) Ambler, R. P. *Philos. Trans. R. Soc. London B* **1980**, *289*, 321−331.

(4) Papp-Wallace, K. M.; Taracila, M. A.; Smith, K. M.; Xu, Y.; Bonomo, R. A. *Antimicrob. Agents Chemother.* **2012**, *56*, 4428−4438.

(5) Doi, Y.; O'Hara, J. A.; Lando, J. F.; Querry, A. M.; Townsend, B. M.; Pasculle, A. W.; Muto, C. A. *Emerg. Infect. Dis.* **2014**, *20*, 163−165.

(6) Bebrone, C. *Biochem. Pharmacol.* **2007**, *74*, 1686−1701.

(7) Carfi, A.; Pares, S.; Duee, E.; Galleni, M.; Duez, C.; Frere, J.; Dideberg, O. *EMBO J.* **1995**, *14*, 4914−4921.

(8) Wang, Z.; Fast, W.; Benkovic, S. J. *Biochemistry* **1999**, *38*, 10013−10023.

(9) Garcia-Saez, I.; Hopkins, J.; Papamicael, C.; Franceschini, N.; Amicosante, G.; Rossolini, G. M.; Galleni, M.; Frere, J.-M.; Dideberg, O. *J. Biol. Chem.* **2003**, *278*, 23868−23873.

(10) Ullah, J. H.; Walsh, T. R.; Taylor, I. A.; Emery, D. C.; Verma, C. S.; Gamblin, S. J.; Spenser, J. *J. Mol. Biol.* **1998**, *287*, 125−136.

(11) Toney, J. H.; Hammond, G. G.; Fitzgerald, P. M. D.; Sharma, N.; Balkovec, J. M.; Rouen, G. P.; Olson, S. H.; Hammond, M. L.; Greenlee, M. L.; Gao, Y.-D. *J. Biol. Chem.* **2001**, *276*, 31913−31918.

(12) Docquier, J. D.; Lamotte-Brasseur, J.; Galleni, M.; Amicosante, G.; Frere, J. M.; Rossolini, G. M. *J. Antimicrob. Chemother.* **2003**, *51*, 257−266.

(13) Yong, D.; Toleman, M. A.; Giske, C. G.; Cho, H. S.; Sundman, K.; Lee, K.; Walsh, T. R. *Antimicrob. Agents Chemother.* **2009**, *53*, 5046−5054.

(14) Bonomo, R. A. *Clin. Infect. Dis.* **2011**, *52*, 485−487.

(15) Kumarasamy, K. K.; Toleman, M. A.; Walsh, T. R.; Bagaria, J.; Butt, F.; Balakrishnan, R.; Chaudhary, U.; Doumith, M.; Giske, C. G.; Irfan, S.; Krishnan, P.; Kumar, A. V.; Maharjan, S.; Mushtaq, S.; Noorie, T.; Paterson, D. L.; Pearson, A.; Perry, C.; Pike, R.; Rao, B.; Ray, U.; Sarma, J. B.; Sharma, M.; Sheridan, E.; Thirunarayan, M. A.; Turton, J.; Upadhyay, S.; Warner, M.; Welfare, W.; Livermore, D. M.; Woodford, N. *Lancet Infect. Dis.* **2010**, *10*, 597−602.

(16) Koh, T. H.; Khoo, C. T.; Wijaya, L.; Leong, H. N.; Lo, Y. L.; Lim, L. C.; Koh, T. Y. *Lancet Infect. Dis.* **2010**, *10*, 828.

(17) Cricco, J. A.; Orellano, E. G.; Rasia, R. M.; Ceccarelli, E. A.; Vila, A. J. *Coord. Chem. Rev.* **1999**, *190−192*, 519−535.

(18) Griffin, D. H.; Richmond, T. K.; Sanchez, C.; M?ller, A. J.; Breece, R. M.; Tierney, D. L.; Bennett, B.; Crowder, M. W. *Biochemistry* **2011**, *50*, 9125−9134.

(19) Yang, H.; Aitha, M.; Hetrick, A. M.; Richmond, T. K.; Tierney, D. L.; Crowder, M. W. *Biochemistry* **2012**, *51*, 3839−3847.

(20) Orellano, E. G.; Girardini, J. E.; Cricco, J. A.; Ceccarelli, E. A.; Vila, A. J. *Biochemistry* **1998**, *37*, 10173−10180.

(21) Hu, Z.; Periyannan, G.; Bennett, B.; Crowder, M. W. *J. Am. Chem. Soc.* **2008**, *130*, 14207−14216.

(22) Llarrull, L. I.; Tioni, M. F.; Vila, A. J. *J. Am. Chem. Soc.* **2008**, *130*, 15842−15851.

(23) Tioni, M. F.; Llarrull, L. I.; Poeylaut-Palena, A. A.; Marti, M. A.; Saggu, M.; Periyannan, G. R.; Mata, E. G.; Bennett, B.; Murgida, D. H.; Vila, A. J. *J. Am. Chem. Soc.* **2008**, *130*, 15852−15863.

(24) Thomas, P. W.; Zheng, M.; Wu, S.; Guo, H.; Liu, D.; Xu, D.; Fast, W. *Biochemistry* **2011**, *50*, 10102−10113.

(25) Riley, E. A.; Petros, A. K.; Smith, K. A.; Gibney, B. R.; Tierney, D. L. *Inorg. Chem.* **2006**, *45*, 10016−10018.

(26) Thomas, P. W.; Stone, E. M.; Costello, A. L.; Tierney, D. L.; Fast, W. *Biochemistry* **2005**, *44*, 7559−7565.

(27) Ankudinov, A. L.; Ravel, B.; Rehr, J. J.; Conradson, S. D. *Phys. Rev. B* **1998**, *58*, 7565−7576.

(28) Bennett, B. EPR of Cobalt-Substituted Zinc Enzymes. In *Metals in Biology*; Springer: New York, 2010; Biological Magnetic Resonance Vol. *29*, p 345−370.

(29) Sharma, N. P.; Hajdin, C.; Chandrasekar, S.; Bennett, B.; Yang, K. W.; Crowder, M. W. *Biochemistry* **2006**, *45*, 10729−10738.

(30) Garrity, J. D.; Bennett, B.; Crowder, M. W. *Biochemistry* **2005**, *44*, 1078−1087.

(31) Crowder, M. W.; Yang, K.-W.; Carenbauer, A. L.; Periyannan, G.; Seifert, M. E.; Rude, N. E.; Walsh, T. R. *J. Biol. Inorg. Chem.* **2001**, *6*, 91−99.

(32) Llarrull, L. I.; Tioni, M. F.; Kowalski, J.; Bennett, B.; Vila, A. J. *J. Biol. Chem.* **2007**, *282*, 30586−30595.

(33) Breece, R. M.; Llarrull, L. I.; Tioni, M. F.; Vila, A. J.; Tierney, D. L. *J. Inorg. Biochem.* **2011**, *111*, 182−186.

(34) Hawk, M. J.; Breece, R. M.; Hajdin, C. E.; Bender, K. M.; Hu, Z.; Costello, A. L.; Bennett, B.; Tierney, D. L.; Crowder, M. W. *J. Am. Chem. Soc.* **2009**, *131*, 10753−10762.

(35) Yamaguchi, Y.; Imamura, K.; Sasao, A.; Murakami, E.; Arakawa, Y.; Kurosaki, H. *Med. Chem. Commun.* **2011**, *2*, 720−725.

(36) Garmer, D. R.; Krauss, M. *J. Am. Chem. Soc.* **1993**, *115*, 10247−10257.

(37) Bicknell, R.; Hanson, G. R.; Holmquist, B.; Little, C. *Biochemistry* **1986**, *25*, 4219−4223.

(38) Crowder, M. W.; Wang, Z.; Franklin, S. L.; Zovinka, E. P.; Benkovic, S. J. *Biochemistry* **1996**, *35*, 12126−12132.

(39) deSeny, D.; Heinz, U.; Wommer, S.; Kiefer, M.; Meyer-Klaucke, W.; Galleni, M.; Frere, J. M.; Bauer, R.; Adolph, H. W. *J. Biol. Chem.* **2001**, *276*, 45065−45078.

(40) Badarau, A.; Damblon, C.; Page, M. I. *Biochem. J.* **2007**, *401*, 197−203.

(41) Bertini, I.; Lanini, G.; Luchinat, C. *J. Am. Chem. Soc.* **1983**, *105*, 5116−5118.

(42) González, J. M.; Meini, M.-R.; Tomatis, P. E.; Martín, F. J. M.; Cricco, J. A.; Vila, A. J. *Nat. Chem. Biol.* **2012**, *8*, 698−700.

(43) Reid, T. S.; Terry, K. L.; Casey, P. J.; Beese, L. S. *J. Mol. Biol.* **2004**, *343*, 417−433.

(44) Huang, C. C.; Casey, P. J.; Fierke, C. A. *J. Biol. Chem.* **1997**, *272*, 20−23.

(45) Periyannan, G.; Costello, A. L.; Tierney, D. L.; Yang, K.-W.; Bennett, B.; Crowder, M. W. *Biochemistry* **2006**, *45*, 1313−20.

(46) Piccioli, M.; Luchinat, C.; Mizoguchi, T. J.; Ramirez, B. E.; Gray, H. B.; Richards, J. H. *Inorg. Chem.* **1995**, *34*, 737−742.

(47) Dennison, C.; Sato, K. *Inorg. Chem.* **2004**, *43*, 1502−1510.

(48) Vila, A. J.; Fernandez, C. O. *J. Am. Chem. Soc.* **1996**, *118*, 7291−7298.

(49) Salgado, J.; Jimenez, H. R.; Donaire, A.; Moratal, J. M. *Eur. J. Biochem.* **1995**, *231*, 358−69.

(50) Banci, L.; Bertini, l.; Luchinat, C.; Viezzoli, M. S. *Inorg. Chem.* **1990**, *29*, 1438−1440.

(51) Renault, J. P.; Verchere-Beaur, C.; Morgenstern-Badarau, I.; Piccioli, M. *FEBS Lett.* **1997**, *401*, 15−19.

(52) Vila, A. J.; Ramirez, B. E.; Di Bilio, A. J.; Mizoguchi, T. J.; Richards, J. H.; Gray, H. B. *Inorg. Chem.* **1997**, *36*, 4567−4570.

(53) Fernandez, C. O.; Sannazzaro, A. I.; Vila, A. J. *Biochemistry* **1997**, *36*, 10566−70.
(54) Donaire, A.; Jimenez, B.; Moratal, J. M.; Hall, J. F.; Hasnain, S. S. *Biochemistry* **2001**, *40*, 837−846.
(55) Donaire, A.; Salgado, J.; Moratal, J. M. *Biochemistry* **1998**, *37*, 8659−8673.
(56) Dennison, C.; Sato, K. *Inorg. Chem.* **2002**, *41*, 6662−6672.
(57) Bertini, I.; Luchinat, C.; Messori, L.; Monnanni, R.; Auld, D. S.; Riordan, J. F. *Biochemistry* **1988**, *27*, 8318−8325.
(58) Bertini, I.; Monnanni, R.; Pellacani, G. C.; Sola, M.; Vallee, B. L.; Auld, D. S. *J. Inorg. Biochem.* **1988**, *32*, 13−20.
(59) Bertini, I.; Turano, P.; Vila, A. J. *Chem. Rev.* **1993**, *93*, 2833−2932.
(60) Momb, J.; Thomas, P. W.; Breece, R. M.; Tierney, D. L.; Fast, W. *Biochemistry* **2006**, *45*, 13385−13393.
(61) Copick, A. J.; Waterson, S.; Swierczek, S. I.; Bennett, B.; Holz, R. C. *Inorg. Chem.* **2005**, *44*, 1160−1162.
(62) Huntington, K. M.; Bienvenue, D. L.; Wei, Y. M.; Bennett, B.; Holz, R. C.; Pei, D. H. *Biochemistry* **1999**, *38*, 15587−15596.
(63) Bienvenue, D. L.; Bennett, B.; Holz, R. C. *J. Inorg. Biochem.* **2000**, *78*, 43−54.
(64) Park, H.; Brothers, E. N.; Merz, K. M. *J. Am. Chem. Soc.* **2005**, *127*, 4232−4241.
(65) Xu, D.; Guo, H.; Cui, Q. *J. Am. Chem. Soc.* **2007**, *129*, 10814−10822.
(66) King, D.; Strynadka, N. *Protein Sci.* **2011**, *20*, 1484−1491.
(67) Strynadka, N. C. J.; King, D. T. *J. Am. Chem. Soc.* **2012**, *134*, 11362−11365.
(68) Zhang, H.; Hao, Q. *FASEB J.* **2011**, 2574−2582.
(69) Crisp, J.; Conners, R.; Garrity, J. D.; Carenbauer, A. L.; Crowder, M. W.; Spencer, J. *Biochemistry* **2007**, *46*, 10664−10674.
(70) Garrity, J. D.; Pauff, J. M.; Crowder, M. W. *J. Biol. Chem.* **2004**, *279*, 39663−39670.
(71) Spencer, J.; Clark, A. R.; Walsh, T. R. *J. Biol. Chem.* **2001**, *276*, 33638−33644.
(72) Stamper, C.; Bennett, B.; Edwards, T.; Holz, R. C.; Ringe, D.; Petsko, C. *Biochemistry* **2001**, *40*, 7035−7046.
(73) Saini, A.; Bansal, R. *Adv. Biol. Chem.* **2012**, *2*, 323−334.
(74) Hernandez, V.; Crepin, T.; Palencia, A.; Cusack, S.; Akama, T.; Baker, S. J.; Bu, W.; Feng, L.; Freund, Y. R.; Liu, L.; Meewan, M.; Mohan, M.; Mao, W.; Rock, F. L.; Sexton, H.; Sheoran, A.; Zhang, Y.; Zhang, Y.-K.; Zhou, Y.; Nieman, J. A.; Anugula, M. R.; Keramane, E. M.; Savariraj, K.; Reddy, D. S.; Sharma, R.; Subedi, R.; Singh, R.; O'Leary, A.; Simon, N. L.; De, M. P. L.; Mushtaq, S.; Warner, M.; Livermore, D. M.; Alley, M. R. K.; Plattner, J. J. *Antimicrob. Agents Chemother.* **2013**, *57*, 1394−1403.
(75) Thakur, P. K.; Kumar, J.; Ray, D.; Anjum, F.; Hassan, M. I. *J. Nat. Sci., Biol. Med.* **2013**, *4*, 51−56.
(76) Zhu, K.; Lu, J.; Ye, F.; Jin, L.; Kong, X.; Liang, Z.; Chen, Y.; Yu, K.; Jiang, H.; Li, J.-Q.; Luo, C. *Biochem. Biophys. Res. Commun.* **2013**, *431*, 2−7.
(77) Livermore, D. M.; Mushtaq, S.; Morinaka, A.; Ida, T.; Maebashi, K.; Hope, R. *J. Antimicrob. Chemother.* **2013**, *68*, 153−158.
(78) Yuan, Q.; He, L.; Ke, H. *Antimicrob. Agents Chemother.* **2012**, *56*, 5157−5163.
(79) Docobo-Perez, F.; Nordmann, P.; Dominguez-Herrera, J.; Lopez-Rojas, R.; Smani, Y.; Poirel, L.; Pachon, J. *Int. J. Antimicrob. Agents* **2012**, *39*, 251−254.
(80) Worthington, R. J.; Bunders, C. A.; Reed, C. S.; Melander, C. *ACS Med. Chem. Lett.* **2012**, *3*, 357−361.
(81) Zheng, B.; Tan, S.; Gao, J.; Han, H.; Liu, J.; Lu, G.; Liu, D.; Yi, Y.; Zhu, B.; Gao, G. F. *Protein Cell* **2011**, *2*, 250−258.
(82) Li, T.; Wang, Q.; Chen, F.; Li, X.; Luo, S.; Fang, H.; Wang, D.; Li, Z.; Hou, X.; Wang, H. *PLoS One* **2013**, *8*, e61914.
(83) Kim, Y.; Cunningham, M. A.; Mire, J.; Tesar, C.; Sacchettini, J.; Joachimiak, A. *FASEB J.* **2013**, *27*, 1−11.
(84) Sharma, N.; Hu, Z.; Crowder, M. W.; Bennett, B. *J. Am. Chem. Soc.* **2008**, *130*, 8215−8222.
(85) Prescott, J. M.; Wagner, F. W.; Holmquist, B.; Vallee, B. L. *Biochemistry* **1985**, *24*, 5350−5356.
(86) Wang, Z.; Fast, W.; Benkovic, S. J. *J. Am. Chem. Soc.* **1998**, *120*, 10788−10789.
(87) Lisa, M. N.; Hemmingsen, L.; Vila, A. J. *J. Biol. Chem.* **2010**, *285*, 4570−4577.
(88) McManus-Munoz, S.; Crowder, M. W. *Biochemistry* **1999**, *38*, 1547−1553.